esearch
nada

Conseil national
de recherches Canada

NRC·CNRC

Canadian
Journal of
Civil Engineering

Revue
canadienne
de génie civil

Volume 31, Number 5, October 2004

Volume 31, numéro 5, octobre 2004

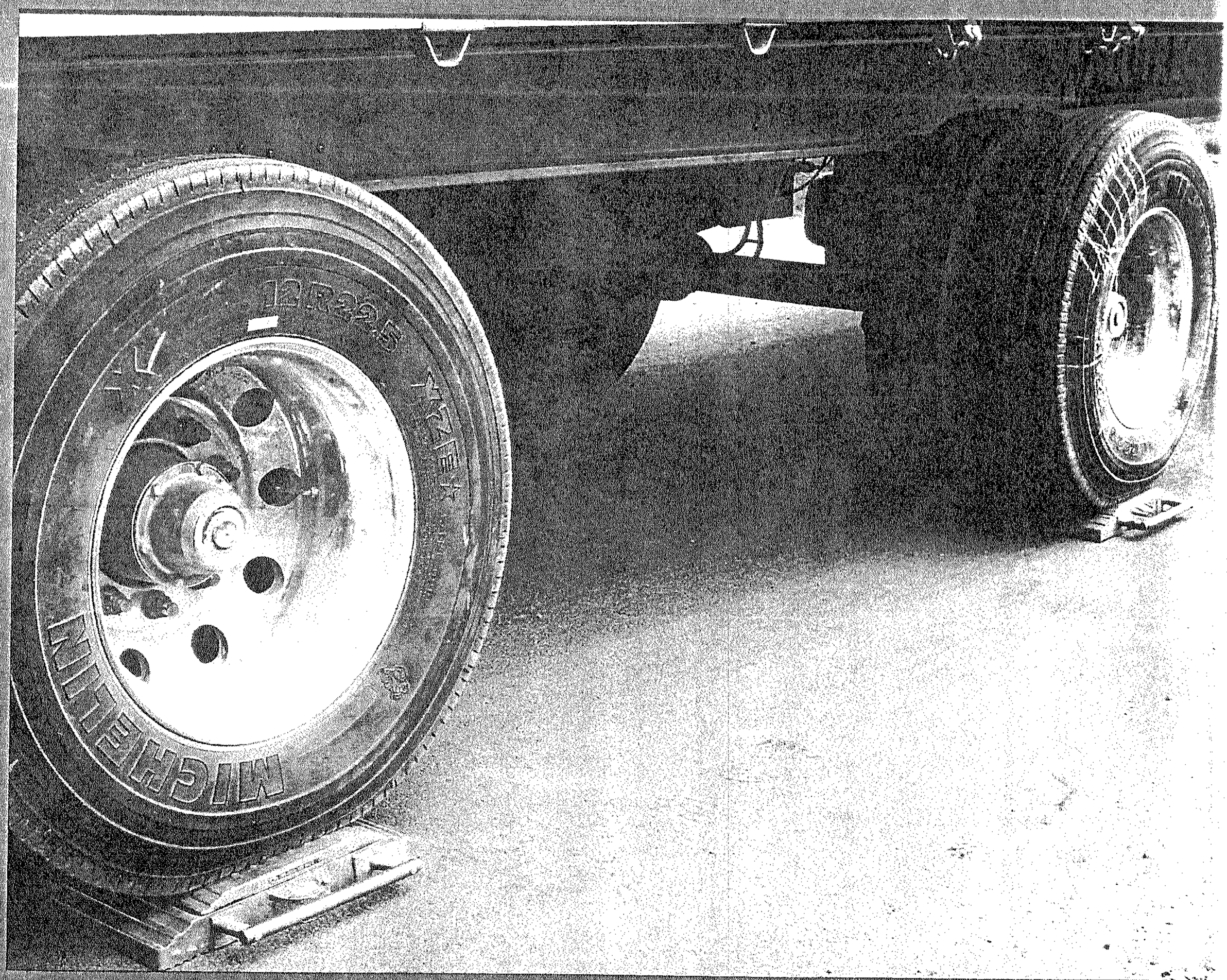

http://cjce.nrc.ca

http://rcgc.cnrc.ca

Parameter studies and verifications on three-dimensional finite element analysis of rigid pavements

Ying-Haur Lee, Hsin-Ta Wu, and Shao-Tang Yen

Abstract: The main objective of this study was to conduct in-depth parameter studies and verifications on three-dimensional (3-D) finite element (FEM) analysis of rigid pavements. A systematic analytical approach was utilized and implemented in a Visual Basic software package to study the effects of mesh fineness and element selection. The deflection and stress convergence characteristics of various 3-D shell and solid elements were investigated. Several guidelines in mesh fineness and element selection were developed and recommended. Using the principles of dimensional analysis, an additional dimensionless variable (h/a, where h is the thickness of the slab and a is the radius of the applied load) was identified and verified to have a substantial influence on ABAQUS runs using either 3-D shell elements or 3-D solid elements. Separate 3-D FEM stress and deflection databases were developed using all dimensionless variables. An example critical stress predictive model was developed. Together with the existing two-dimensional FEM research findings, a tentative stress prediction equation was proposed to illustrate its possible applications.

Key words: rigid pavement, finite element model, stress, deflection, design, evaluation.

Résumé : L'objectif principal de la présente étude est d'étudier en profondeur les paramètres et d'effectuer des vérifications de l'analyse tridimensionnelle par éléments finis des chaussées rigides. Une approche analytique systématique a été utilisée et implantée dans un logiciel en Visual Basic afin d'étudier les effets de la finesse des mailles et de la sélection des éléments. Les caractéristiques de flexion et de convergence des contraintes de divers éléments pleins et d'enveloppes tridimensionnels ont été étudiées. En utilisant les principes d'analyse dimensionnelle, une variable additionnelle sans dimension (h/a) a été identifiée et il a été confirmé qu'elle avait une influence substantielle sur les passages d'ABAQUS utilisant soit l'enveloppe tridimensionnelle ou les éléments pleins tridimensionnels. Des bases de données séparées sur la flexion et la contrainte selon une méthode par éléments finis tridimensionnels ont été développées en utilisant toutes les variables sans dimensions. Un exemple d'un modèle de prévision des contraintes critiques a été développé. En combinaison avec les conclusions existantes de recherche par une méthode par éléments finis bidimensionnels, une équation provisoire de prédiction des contraintes est proposée afin d'en illustrer les utilisations possibles.

Mots clés : chaussée rigide, modèle d'éléments finis, contrainte, flexion, conception, évaluation.

[Traduit par la Rédaction]

Introduction

Determination of critical structural responses in terms of stresses and deflections in a concrete slab is essential to mechanistic-based design and structural evaluation procedures. Two-dimensional (2-D, ILLI-SLAB) finite element models (FEMs) have been successfully utilized to account for the effects of many practical pavement conditions more realistically than theoretical solutions based on infinite slab and full contact assumptions. The applicability of the ILLI-SLAB program for stress estimation has been previously investigated through comparisons of the resulting stresses and the actual field measurements from some test sections of Taiwan's second northern highway, the American Association of State Highway Officials (AASHO) road test, and the Arlington road test with reasonably good agreements (Lee 1999). With the introduction of three-dimensional (3-D, ABAQUS) FEMs and all the promising features and results reported in the literature (Kuo 1994; Brill 1998; Hammons 1998; Kim and Hjelmstad 2000; Thompson and Navneet 1999), its applications in pavement engineering becomes inevitable. Nevertheless, because of the required running time and the complexity of FEM, 3-D finite element analysis cannot be easily implemented as a part of the design or structural evaluation procedure. Thus, the main objective of this study was to conduct in-depth parameter studies and verifications on 3-D finite element analysis of rigid pavements (Wu 2003).

A single slab resting on a Winkler foundation with three critical loading conditions was considered. To study the effects of mesh fineness and element selection on the results

Received 10 October 2003. Revision accepted 11 May 2004. Published on the NRC Research Press Web site at http://cjce.nrc.ca on 6 October 2004.

Y.-H. Lee,[1] H.-T. Wu, and S.-T. Yen. Department of Civil Engineering, Tamkang University, E725, #151 Ying-Chuan Road, Tamsui, Taipei, Taiwan 251

[1]Corresponding author (e-mail: yinghaur@mail.tku.edu.tw).

Written discussion of this article is welcomed and will be received by the Editor until 28 February 2005.

of FEM runs, a systematic analytical approach was utilized and implemented in a Visual Basic software package to automatically construct FEMs, generate the input files, conduct the runs, and summarize the results. Several guidelines in mesh fineness and the selection of various element types were subsequently developed. The principles of dimensional analysis were utilized throughout this study. Besides the normalized load radius (a/l, where a is the radius of the applied load and l is the radius of relative stiffness of the slab–subgrade system), the normalized finite slab length (L/l, where L is the finite slab length), and the normalized finite slab width (W/l, where W is the finite slab width), an additional dominating dimensionless variable (h/a) defined as the ratio of slab thickness (h) to load radius (a) was identified and verified to have a substantial influence on ABAQUS runs using either 3-D shell elements or 3-D solid elements. This additional mechanistic variable can be used to account for the differences among various 2-D and 3-D FEM idealizations and theoretical closed-form stress and deflection solutions.

Separate stress and deflection databases were created using these dimensionless mechanistic variables. Example predictive models in terms of adjustment factors of critical stresses and deflections in a concrete slab were developed to illustrate their possible applications. The ultimate goal of this study is to bridge the gap between various 2-D and 3-D FEM idealizations and closed-form solutions to develop a new mechanistic-based design procedure using the results of 3-D FEM analysis.

Closed-form solutions and finite element idealizations

Based on the assumption of an infinite or semi-infinite slab over a dense liquid (Winkler) foundation, Westergaard obtained the following closed-form solutions subjected to a single edge, interior, and corner wheel load (Ioannides et al. 1985):

$$\sigma_{we} = \frac{3(1+\mu)P}{\pi(3+\mu)h^2}\left[\ln\frac{Eh^3}{100ka^4} + 1.84 - \frac{4}{3}\mu + \frac{1-\mu}{2} + 1.18(1+2\mu)\frac{a}{l}\right]$$

$$\sigma_{wi} = \frac{3(1+\mu)P}{2\pi h^2}\left[\ln\frac{2l}{a} - \gamma + 0.5 + \frac{\pi}{32}\left(\frac{a}{l}\right)^2\right]$$

[1] $$\sigma_{wc} = \frac{3P}{h^2}\left[1 - \left(\sqrt{2}\frac{a}{l}\right)^{0.6}\right]$$

$$\delta_{we} = \frac{\sqrt{2+1.2\mu}P}{\sqrt{Eh^3k}}\left[1 - \frac{(0.76+0.4\mu)a}{l}\right]$$

$$\delta_{wi} = \frac{P}{8kl^2}\left[1 + \frac{1}{2\pi}\left(\ln\frac{a}{2l} - 0.673\right)\left(\frac{a}{l}\right)^2\right]$$

$$\delta_{wc} = \frac{P}{kl^2}\left[1.1 - 0.88\left(\sqrt{2}\frac{a}{l}\right)\right]$$

where σ_{we}, σ_{wi}, and σ_{wc} are Westergaard's closed-form edge, interior, and corner stress solutions, respectively [FL^{-2}]; δ_{we}, δ_{wi}, and δ_{wc} are the edge, interior, and corner deflections, respectively [L]; P is the single wheel load [F]; h is the thickness of the slab [L]; a is the radius of the applied load [L]; $l = \{Eh^3/[12(1-\mu^2)k]\}^{0.25}$ is the radius of relative stiffness of the slab–subgrade system [L]; k is the modulus of subgrade reaction [FL^{-3}]; E is the concrete modulus of the slab [FL^{-2}]; μ is Poisson's ratio; and $\gamma = 0.5772$ is Euler's constant. Note that the primary dimension for force is represented by [F], and length is represented by [L].

The analysis of finite slab length and width was not possible until the introduction of FEMs. The well-known ILLI-SLAB (2-D) and ABAQUS (3-D) FEMs were selected for this study (Korovesis 1990; Hibbitt, Karlsson, & Sorensen, Inc. 2000). Table 1 contains a brief summary of the characteristics of the ILLI-SLAB finite element and 3-D shell and solid elements from the ABAQUS library considered in this study (Kuo 1994; Hammons 1998; Wu 2003). These include both linear and quadratic elements employing both full and reduced integration. The number of nodes, the degrees of freedom, and the number of Gauss integration points per element indicating their relative complexity and required computation time are also summarized. As shown in Figs. 1*a*–1*c*, different types of thin shell elements (four-node, eight-node, and nine-node) are considered, including those satisfying the thin shell theory (the Kirchhoff constraint) analytically and those converging to the thin shell theory numerically as the thickness decreases. The selected 3-D solid (brick) elements (eight-node, 20-node, and 21- to 27-node) include first-order (linear) and second-order (quadratic) interpolation elements as shown in Figs. 1*d*–1*f*. Second-order elements provide higher accuracy than first-order elements and are very effective in bending-dominated problems.

The element types S4 and S4R are general-purpose shells. The S4R5, S8R5, and S9R5 shell elements, which impose the Kirchhoff constraint numerically, are intended for the analysis of thin shells, whereas the element type S8R should be used only for thick shells. Element type C3D20 has 27 integration points, whereas C3D20R has only eight integration points. The C3D27 and C3D27R elements are variable-node elements, of which the number of nodes can be reduced to 21 (or any number between 21 and 27) per element by removing the interior node from each of the faces of the element as desired (Hibbitt, Karlsson, & Sorensen, Inc. 2000).

Reduced integration reduces the computation time through the use of a lower order integration to form the element stiffness. Generally speaking, the accuracy achieved with full versus reduced integration first-order elements is largely dependent on the nature of the problem. For second-order elements, reduced-integration elements generally yield more accurate results than the corresponding fully integrated elements (Hammons 1998; Hibbitt, Karlsson, & Sorensen, Inc. 2000).

Parameter analysis and model building

Definition of mesh fineness and mesh generation

Mesh generation in the horizontal direction as shown in Fig. 2 generally includes the following steps: consideration of applicable symmetry option, generation of finer mesh at

Table 1. Characteristics of ILLI-SLAB element, ABAQUS 3-D shell elements, and ABAQUS 3-D solid elements.

Name	No. of nodes	Degrees of freedom	Reduced integration	Interpolation	No. of gauss points
ILLI-SLAB					
RPB12	4	3	No	Linear	4
ABAQUS 3-D shell elements					
S4	4	6	No	Linear	4
S4R	4	6	Yes	Linear	1
S4R5	4	5	Yes	Linear	1
S8R	8	6	Yes	Quadratic	4
S8R5	8	5	Yes	Quadratic	4
S9R5	9	5	Yes	Quadratic	4
ABAQUS 3-D solid elements					
C3D8	8	3	No	Linear	8
C3D8R	8	3	Yes	Linear	1
C3D20	20	3	No	Quadratic	27
C3D20R	20	3	Yes	Quadratic	8
C3D27	21–27	3	No	Quadratic	27
C3D27R	21–27	3	Yes	Quadratic	14

the loaded area (zone I) and at its neighborhood area (zone II), and progressive increase to coarser mesh farther away (zone III) for efficiency consideration. Throughout this study, horizontal mesh fineness is defined as the ratio of the length of the loaded area to the selected element length. In addition, zones I and II were chosen to have the same mesh fineness, whereas the mesh of zone III was chosen to be four times coarser than that in zone I according to previous literature (Ioannides 1984). The length of the neighborhood area (nC, where n is a multiplier and C is the length of the loaded area) will be further investigated, though it was usually selected as twice the length of the loaded area (C). Although there are some controversies regarding mesh generation in the vertical direction (Ioannides 1984; Kuo 1994; Hammons 1998), vast amounts of computer resources are required if a certain aspect ratio in the vertical direction, e.g., less than 0.8, is chosen, especially for a small wheel load area and (or) small horizontal mesh length. Thus, it was decided that vertical mesh fineness would be defined as the number of evenly divided layers for practical model building concerns in this study.

Deflection convergence characteristics

A single finite slab resting on a Winkler foundation under three loading conditions (edge, interior, corner) with the following input parameters was chosen for the horizontal mesh fineness study: L = 5.00 m (197 in.), W = 5.00 m (197 in.), E = 8.27 GPa (1.2 Mpsi), h = 21.6 cm (8.5 in.), k = 27 MN/m^3 (100 lb/in.^{3}), tire pressure p = 620 kPa (90 psi), μ = 0.15, and P = 10 kN (2250 lb). According to the principles of dimensional analysis, this is equivalent to a pavement having a/l = 0.1, L/l = 7, W/l = 7, and h/a = 3, to be discussed later. For higher accuracy consideration, the same horizontal mesh fineness of up to 10 for zones I and II was considered, in which the length of zone II was set to eight times the length of the loaded area (C). The slab thickness was subdivided into a maximum of four sublayers for vertical mesh fineness study.

The deflection convergence characteristics of various FEM element types were investigated. For all three loading conditions analyzed, the resulting deflections are generally in the following descending order: ABAQUS 3-D solid elements, ABAQUS 3-D shell elements, ILLI-SLAB element, and Westergaard solutions. The element types S8R, S8R5, and S9R5 resulted in very close deflection solutions. For four-node shell elements, the deflections are in the following order: S4R5 < S4 < S4R when coarser mesh was used. The convergence characteristics of eight- and nine-node elements are more effective than those of four-node elements, and their deflections are generally slightly higher than those of four-node elements. For 3-D solid elements, using a vertical mesh fineness of one (or one layer) proved inadequate. By increasing the horizontal and vertical mesh fineness, the resulting deflections of eight-node solid elements were very close to those of 20- and 27-node elements. Generally speaking, the deflections of all 3-D shell elements and solid elements tend to increase to convergence when a finer horizontal mesh is used. Nevertheless, the deflections of C3D20, C3D20R, and C3D27 tend to increase to convergence, whereas the deflections of C3D8, C3D8R, and C3D27R tend to decrease to convergence for finer vertical mesh, i.e., subdivided into more layers. To achieve high accuracy and computation efficiency, it was recommended that element types C3D20 or C3D27 with a horizontal mesh fineness of three and a vertical mesh fineness of three be selected for further analysis. Figures 3 and 4, which depict the interior deflection convergence characteristics of 3-D shell and 3-D solid elements, respectively, are provided for illustration purposes. The deflection ratio is defined as the ratio of the resulting FEM deflections to the corresponding Westergaard solutions: horizontal mesh fineness = 1–10, and vertical mesh fineness = 1–4.

Stress convergence characteristics

Similarly, the stress convergence characteristics of various element types were subsequently investigated. For all three

Fig. 1. Selected element types including (*a*) four-node, (*b*) eight-node, and (*c*) nine-node shell elements, and (*d*) eight-node, (*e*) 20-node, and (*f*) 21- to 27-node solid elements.

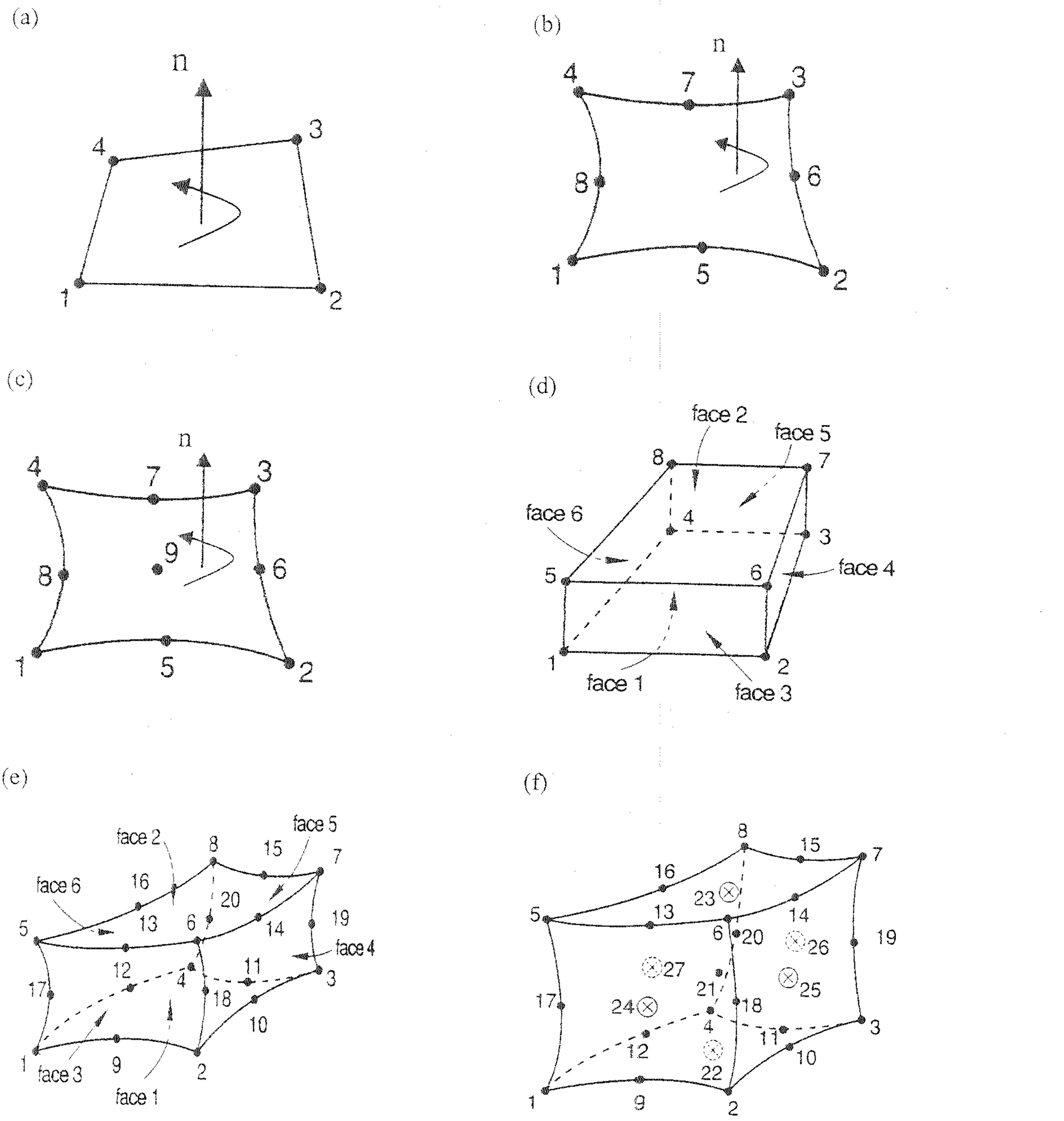

Fig. 2. Illustration of horizontal mesh generation zones (I–III).

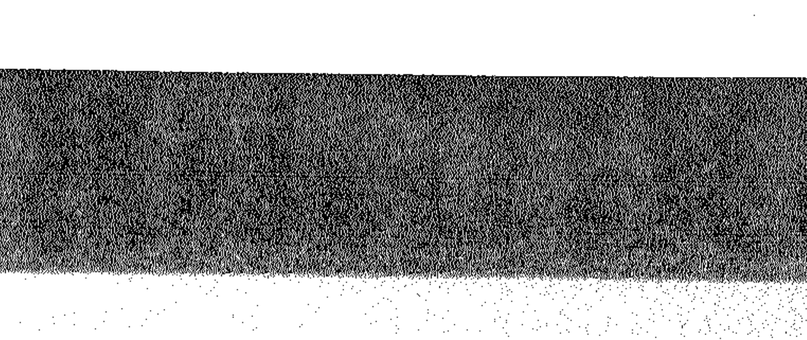

loading conditions analyzed, the stresses of eight- and nine-node shell elements tend to decrease to convergence, whereas those of four-node shell elements increase to convergence when finer horizontal mesh was used. The element types S8R5 and S9R5 resulted in very close stress solutions. Using a vertical mesh fineness of one layer proved inadequate and should be avoided for 3-D solid elements.

Regardless of increasing horizontal and vertical mesh fineness, the resulting stresses of eight-node solid elements are very different from those of 20- and 27-node elements. The interior and edge stresses of element types C3D20 and C3D27 increase to convergence at a faster rate than any other 3-D solid elements when a finer vertical mesh was used. The solid elements with reduced integration resulted in

Fig. 3. Interior deflection convergence characteristics (3-D shell elements).

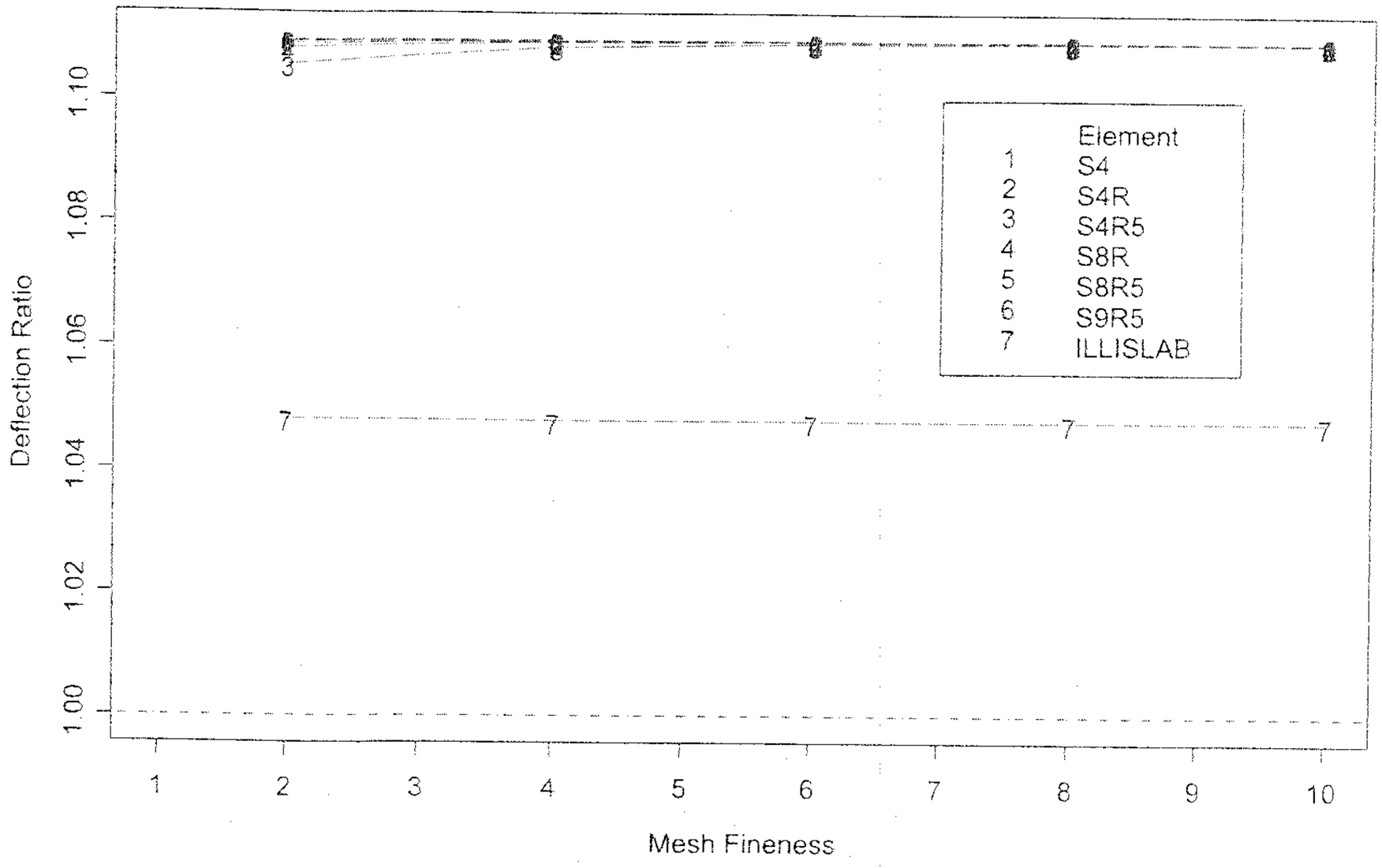

stress reduction of approximately 1% when compared with those without reduced integration. The stresses of 20-node elements were approximately 2% lower than those of 27-point elements when coarser mesh was used. The execution time of 20-point elements is approximately 60% of that of 27-point elements.

Thus, the aforementioned recommendation for selecting element types C3D20 or C3D27 with a horizontal mesh fineness of three and a vertical mesh fineness of three remains unchanged to achieve high accuracy and computation efficiency. Figures 5 and 6 display the edge stress convergence characteristics of 3-D shell and 3-D solid elements, respectively, in which stress ratio is defined as the ratio of the resulting FEM stresses to the corresponding Westergaard solutions; horizontal mesh fineness = 1–10 and vertical mesh fineness = 1–4.

As shown in Fig. 7, however, the corner stresses or the maximum principal tensile stresses at the slab corner had not converged to a certain value, even when element type C3D27 with a very fine horizontal mesh was chosen for a fine vertical mesh of up to four layers. Thus, corner stress analysis using 3-D solid elements may be problematic and should be further investigated because of the poor vertical convergence characteristics of the 3-D solid elements.

Convergence characteristics due to different slab thicknesses and load sizes

The following eight pavement-loading systems were chosen to investigate the effects of different slab thicknesses and load sizes to convergence characteristics: $L/l = 7$; $W/l = 7$; $h/a = 2$ and 4; and $a/l = 0.05$, 0.1, 0.2, and 0.3. Element type C3D27 was chosen for the remaining analyses. The vertical or horizontal mesh fineness was set to three to study the effects of horizontal or vertical mesh fineness (up to 5) to the convergence characteristics of three loading conditions.

Similar deflection convergence characteristics were observed for all systems. The deflections increase to convergence when finer horizontal or vertical mesh is used for all three loading cases. The deflections of a pavement with smaller slab thickness and load size (smaller h/a and a/l) converge faster. By the same token, similar stress convergence patterns were observed. The interior and edge stresses of element type C3D27 decrease to convergence when finer horizontal mesh is used, whereas they increase to convergence when finer vertical mesh or more sublayers are used. The interior and edge stresses of a pavement with smaller h/a and a/l have better convergence characteristics than the other pavement conditions.

The effect of vertical mesh fineness on stress is greater than that of horizontal mesh fineness. The thicker the pavement (larger h/a), the more difficult it is for the corner stress to achieve convergence. The aforementioned recommendation of selecting a horizontal mesh fineness of three and a vertical mesh fineness of three is adequate to achieve good convergence and computation efficiency. Figures 8 and 9 display the edge stress convergence characteristics due to different horizontal and vertical mesh fineness, respectively. Note that stress ratio (1) is the ratio of the resulting ABAQUS stress of any mesh fineness to the stress of the finest mesh used in the analysis, which is slightly different from the stress ratio used in Figs. 5–7.

Determination of the length of neighborhood area

The length of neighborhood area (nC) selected for finer horizontal mesh was further investigated, in which n, ranging from 1 to 8, was selected to study its effects on the results of FEM computation accuracy. The pavement-loading system described previously and having $a/l = 0.1$, $L/l = 7$, $W/l = 7$, and $h/a = 3$ was reanalyzed here. All the aforementioned element types with a horizontal mesh fineness of

Fig. 4. Interior deflection convergence characteristics for (*a*) C3D8, (*b*) C3D8R, (*c*) C3D20, (*d*) C3D20R, (*e*) C3D27, and (*f*) C3D27R element types (3-D solid elements). Note 1–4 stands for the selected vertical mesh fineness, respectively.

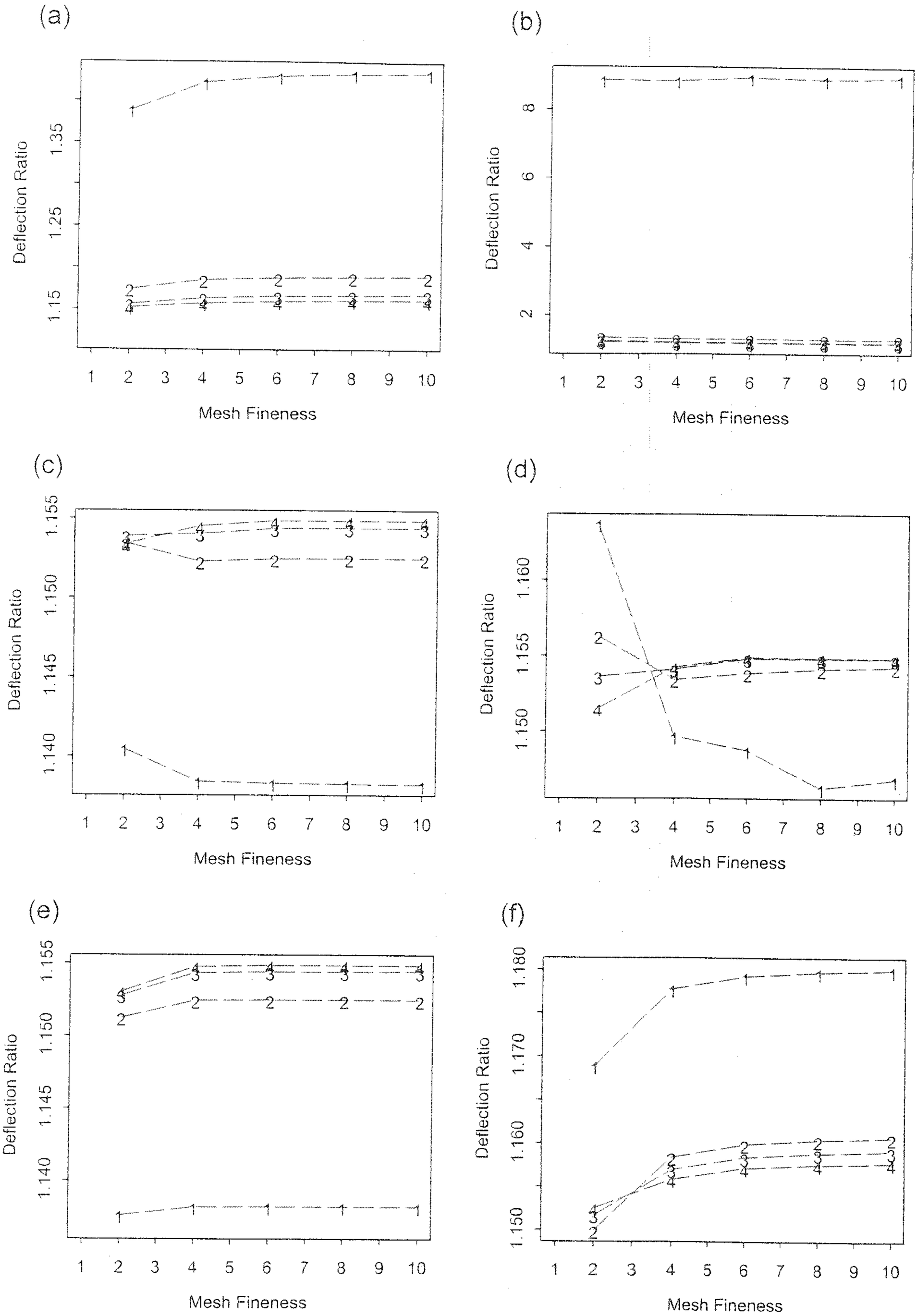

Fig. 5. Edge stress convergence characteristics (3-D shell elements).

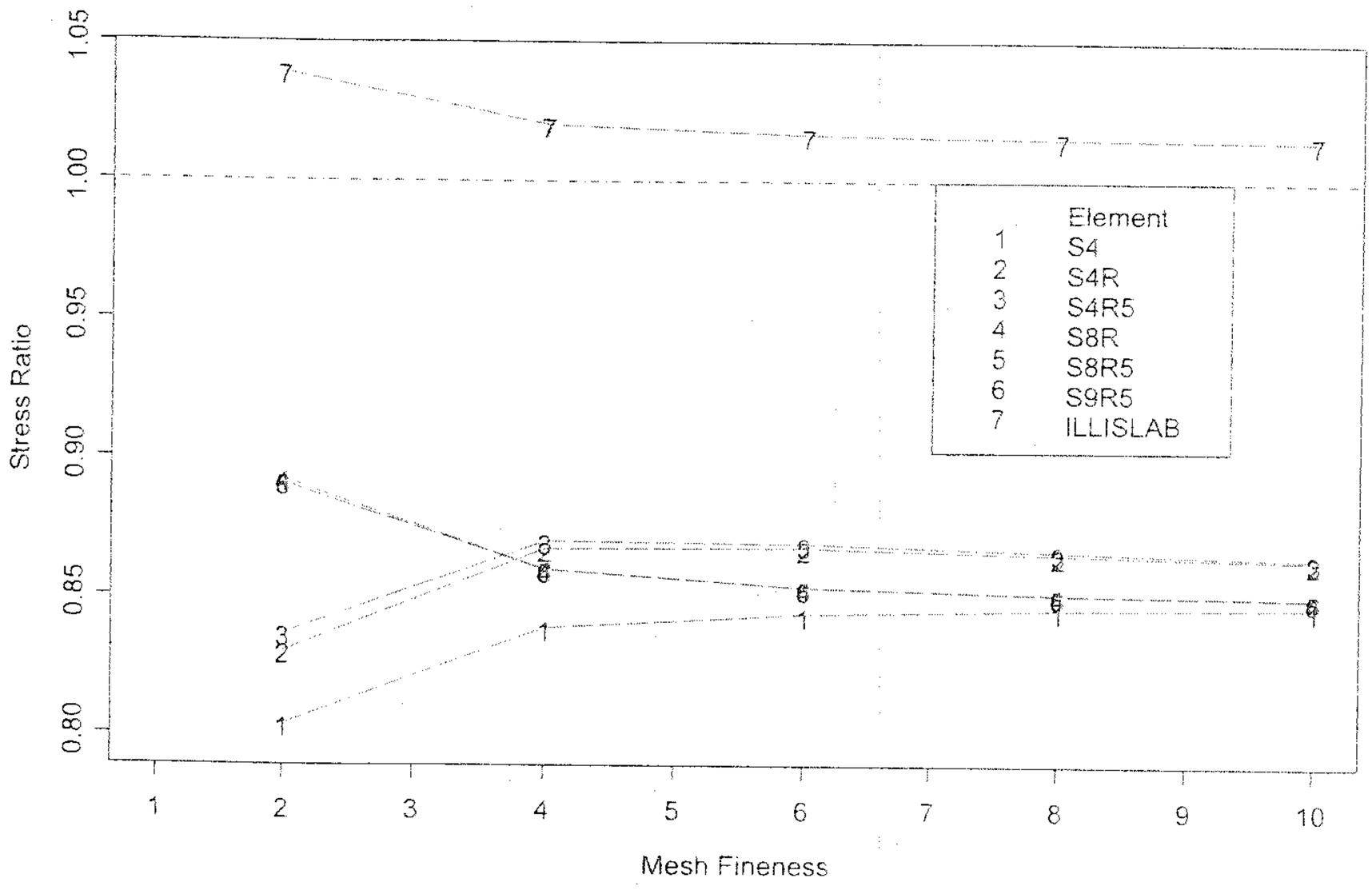

three and a vertical mesh fineness of three were analyzed. The resulting FEM deflections and stresses of any mesh fineness were compared with the corresponding ones with the finest mesh (or eight times the length of the loaded area C).

The deflections and stresses of ILLI-SLAB and four-node elements were affected by the length of zone II. However, the resulting deflections and stresses of eight- and nine-node elements were identical when nC is greater than or equal to two times the length of the loaded area C. Regardless of the different nC values selected, the resulting deflections and stresses of 20- and 27-node solid elements are identical or almost identical. The differences in deflection due to the selection of nC are negligible or up to 0.3%. When nC is greater than or equal to three times C, the differences in the resulting stresses of 3-D shell elements are within 0.2%. Figure 10 depicts the edge stress convergence characteristics. Therefore, a value of three times C is recommended for all element types for consistency and conservative consideration.

Identification of additional dimensionless variable

According to earlier literature, the following relationship has been identified and verified through many 2-D ILLI-SLAB studies for a constant Poisson's ratio (Ioannides et al. 1985; Ioannides and Salsilli-Murua 1989; Salsilli-Murua 1991; Lee 1993):

$$[2] \qquad \frac{\sigma h^2}{P}, \frac{\delta k l^2}{P} = f\left(\frac{a}{l}, \frac{L}{l}, \frac{W}{l}\right)$$

where σ is the slab bending stress, and δ is the slab deflection.

Extreme difficulties were encountered while using only these three dimensionless variables for 3-D FEM analyses. Based on the principles of dimensional analysis, in addition to the normalized load radius (a/l), the normalized finite slab length (L/l), and the normalized finite slab width (W/l), an additional dominating dimensionless variable (h/a) defined as the ratio of slab thickness (h) to load radius (a) was subsequently identified. The following relationship can be used to account for the theoretical differences of various 3-D shell and solid elements:

$$[3] \qquad \frac{\sigma h^2}{P}, \frac{\delta k l^2}{P} = f\left(\frac{a}{l}, \frac{L}{l}, \frac{W}{l}, \frac{h}{a}\right)$$

While keeping these four dimensionless variables constant and changing any other input parameters (a, h, l, L, W, E, k, P), the resulting dimensionless 3-D FEM stresses ($\sigma h^2/P$) and deflections ($\delta k l^2/P$) remained constant. This relationship was numerically verified with the selected element type C3D27 under all three loading cases (interior, edge, and corner). Some results for the identification of an additional dimensionless variable for edge loading analysis are summarized in Table 2. In addition, the relationship given by eq. [3] was further verified for all the aforementioned 3-D shell elements under the interior loading condition with excellent agreements.

The identification of the aforementioned parameter (h/a) was originally inspired by the solutions and charts of Burmister's layered theory for a two-layer system and a three-layer system (Burmister 1943, 1945; Huang 1993). A more in-depth literature survey conducted after the completion of the study by Wu (2003) also indicated that analytical solutions derived for thick elastic plates are governed by the ratio of a circular load radius, a, to the thickness of the slab, h (Shi and Yao 1989; Van Cauwelaert 1990; Ioannides and Khazanovich 1994; Khazanovich and Ioannides 1995), in which different a/h ratios were used to compute the maximum bending stress at the bottom of the slab, σ, in terms of

Fig. 6. Edge stress convergence characteristics for (*a*) C3D8, (*b*) C3D8R, (*c*) C3D20, (*d*) C3D20R, (*e*) C3D27, and (*f*) C3D27R element types (3-D solid elements). Note 1–4 stands for the selected vertical mesh fineness, respectively.

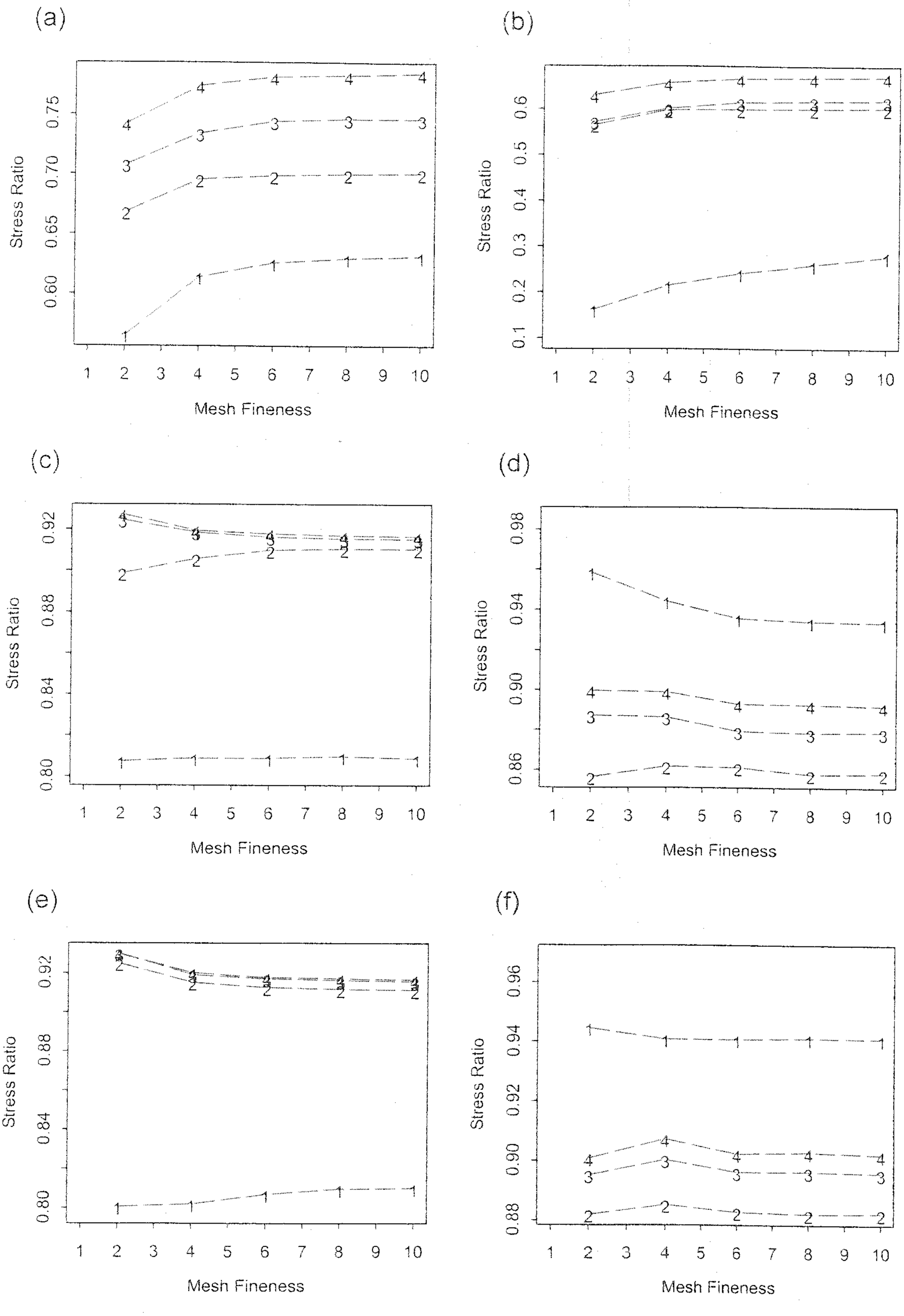

Fig. 7. Corner stress convergence characteristics for (*a*) C3D8, (*b*) C3D8R, (*c*) C3D20, (*d*) C3D20R, (*e*) C3D27, and (*f*) C3D27R element types (3-D solid elements). Note 1–4 stands for the selected vertical mesh fineness, respectively.

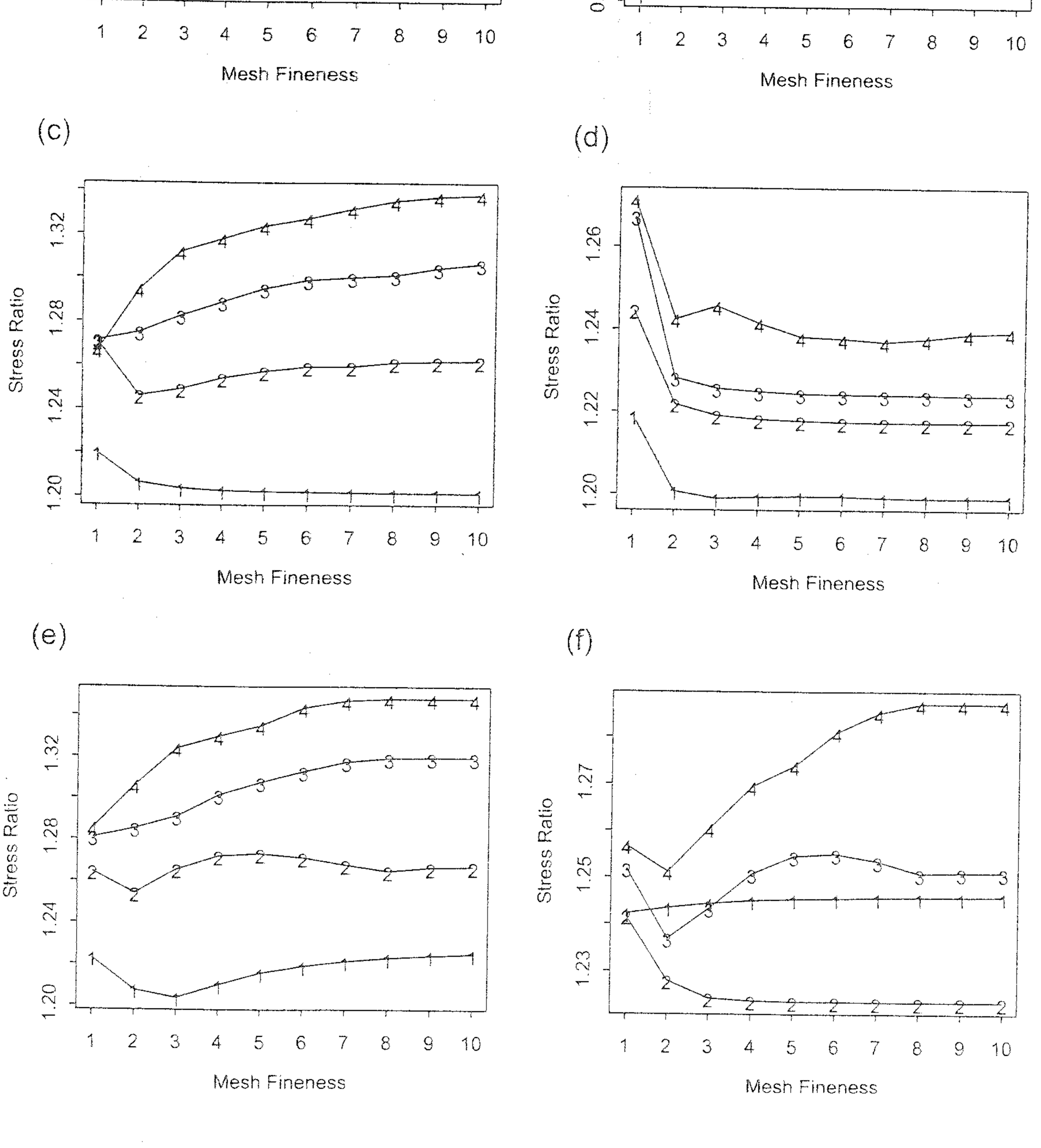

Fig. 8. Horizontal mesh fineness convergence study (edge stress).

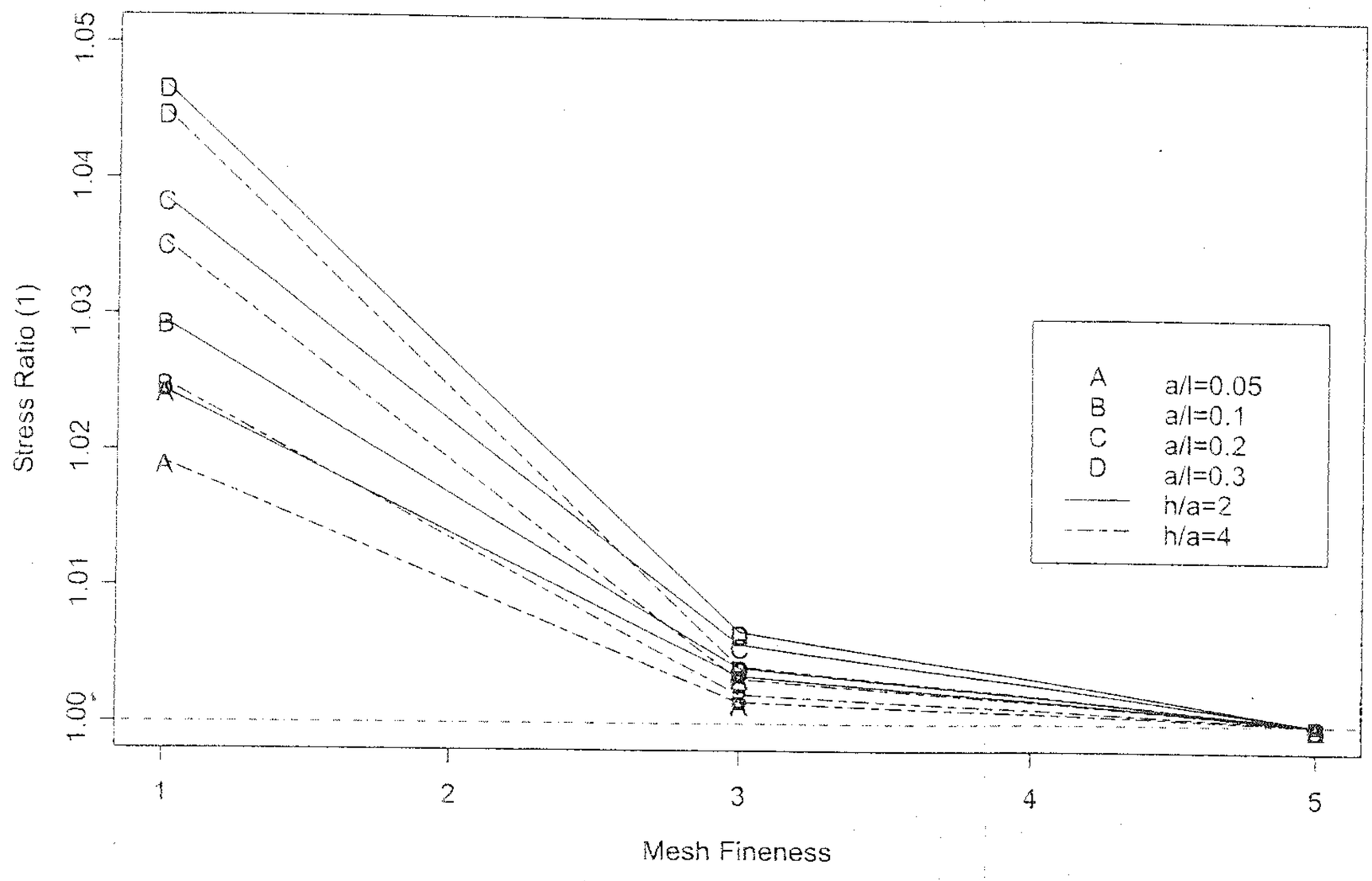

Fig. 9. Vertical mesh fineness convergence study (edge stress).

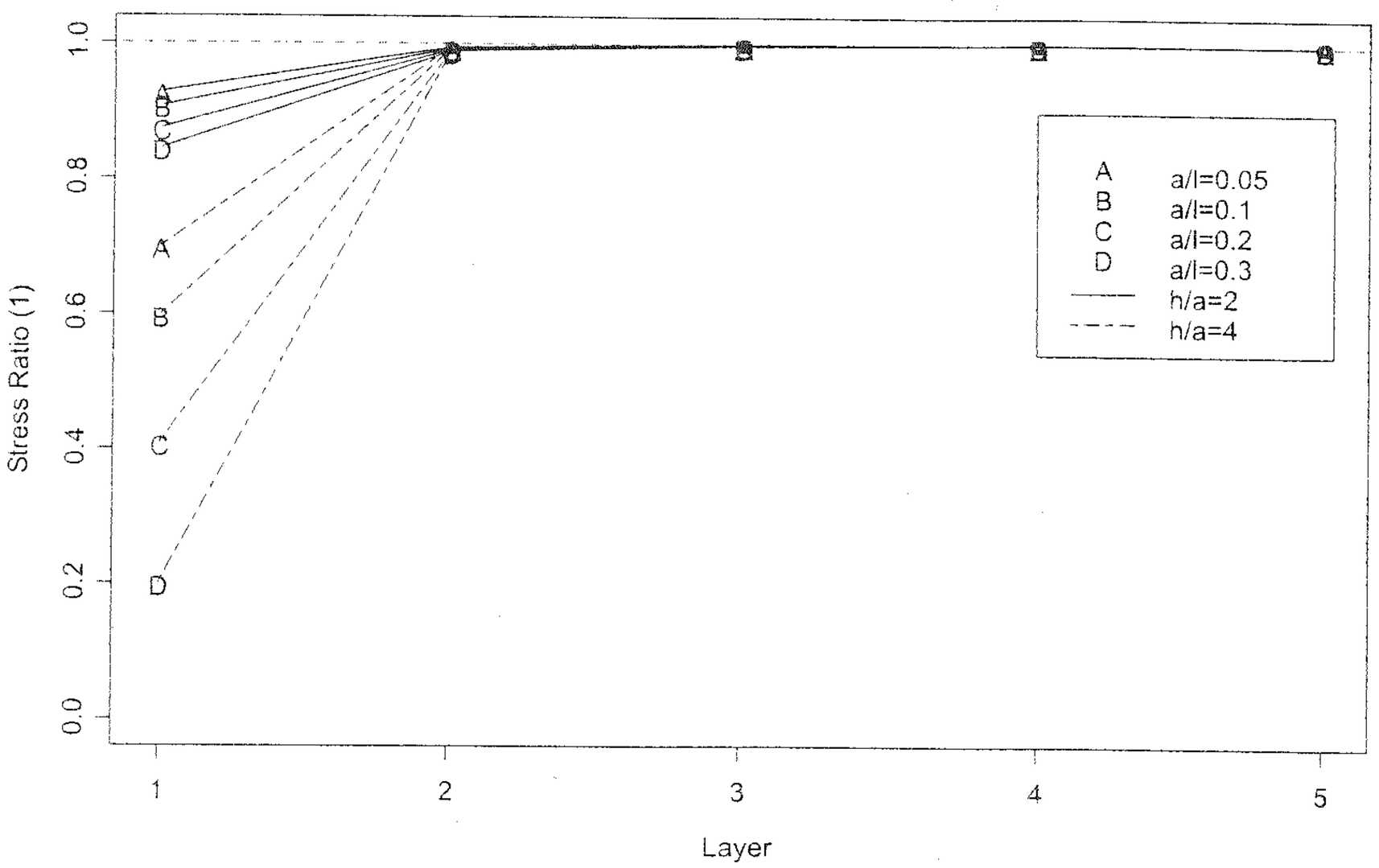

the percentage of the applied pressure, p. The conventional Westergaard's ordinary theory solution results in an overestimate of the bending stress. The correction introduced by Westergaard's special theory results in a reduction in bending stress, bringing it in line with Burmister's layered solutions (Ioannides and Khazanovich 1994).

Development of databases and prediction models

An automated analysis program was developed using the Visual Basic software package to automatically construct FEM models, generate the input files, conduct the runs, and summarize the results. This program was also capable of assisting in conducting all the aforementioned analyses through the selection of different loading locations, various 3-D shell and solid elements, horizontal and vertical mesh fineness, and the length of zone II.

A series of 3-D FEM factorial runs was conducted for a single slab resting on a Winkler foundation with three critical loading conditions based on the following dimensionless parameters: L/l = 2–7 (step by 1); a/l = 0.05, 0.1–0.5 (step by 0.1); h/a = 0.5–6.0 (step by 0.5); and W/l = L/l. These ranges were carefully selected to cover a very wide range of

Fig. 10. Edge stress convergence study due to the length of neighborhood area.

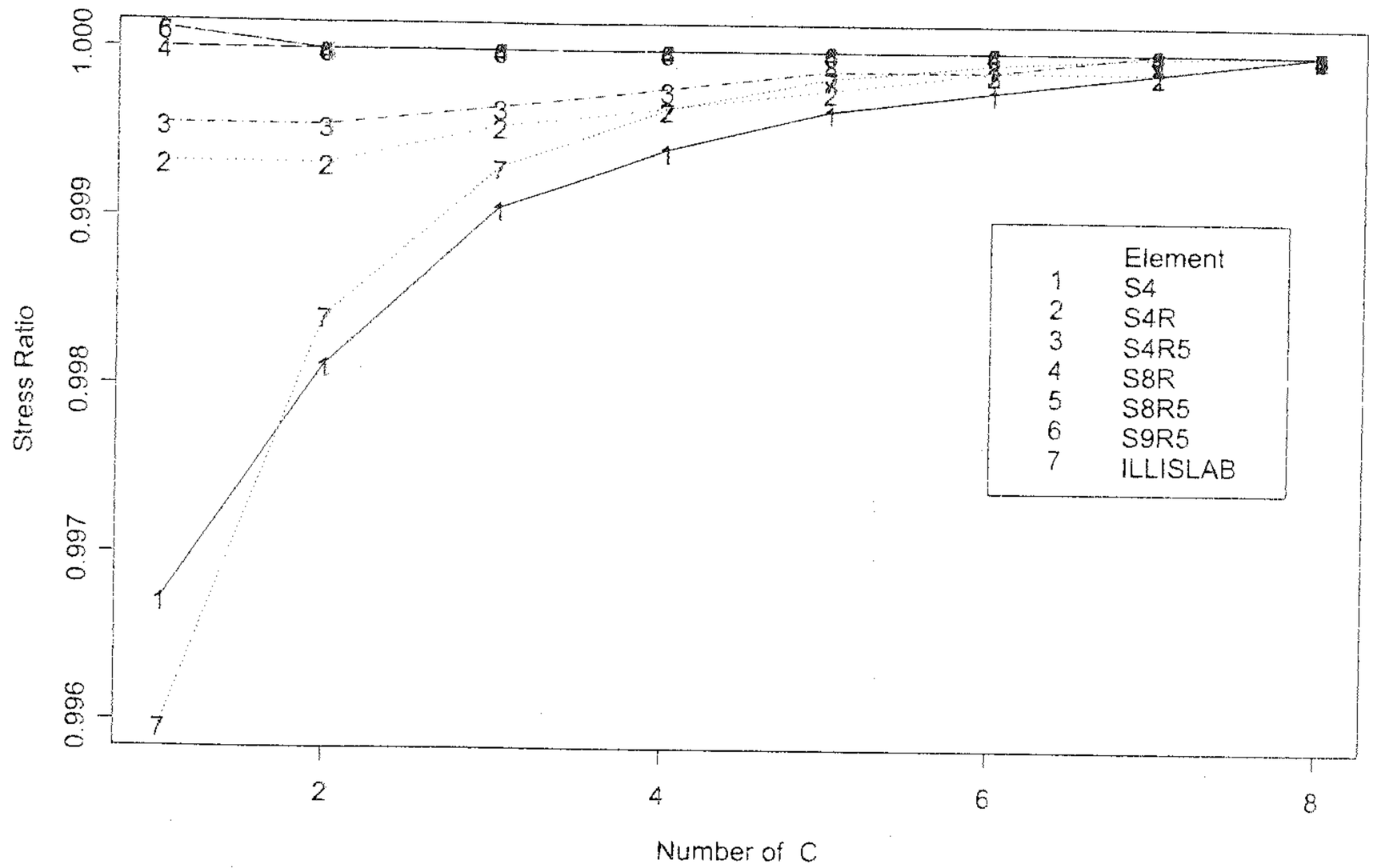

highway and airfield rigid pavement conditions. Separate deflection and stress databases were created for all three loading conditions using element type C3D27 with a horizontal mesh fineness of three, a vertical mesh fineness of three, and the same finer mesh extended to three times the length of the loaded area (C).

Deflection ratios and stress ratios defined as the ratio of 3-D finite element results to Westergaard solutions were calculated while assuming the normalized slab width W/l equals L/l, i.e., square slabs. Note that Westergaard's closed-form solutions only serve as benchmarks herein instead of "exact solutions," since the solutions are based on the simplification that ignores plate compressibility and shear deformation. Since the resulting deflection ratios always had a value greater than 1, their reciprocals or adjustment factors (R) will range from 0 to 1. The very high deflection ratios occurred when a thicker pavement (larger h/a) or a larger load size (larger a/l) was analyzed. Similarly, the resulting edge stress ratios ranged from 0.25 to 1.03.

To illustrate possible applications of these databases, the following predictive model was developed for critical edge stress estimation using the projection pursuit regression technique (Lee and Darter 1994; Friedman and Stuetzle 1981):

$$R_{3\text{-D}} = \frac{\sigma_{3\text{-D FEM}}}{\sigma_{we}} = f\left(\frac{a}{l}, \frac{L}{l}, \frac{h}{a}\right)$$

$$R_{3\text{-D}} = 0.69149 + 0.259\Phi_1 + 0.03318\Phi_2$$

$$\Phi_1 = \begin{cases} 1.578 + 6.013(A_1) + 2.673(A_1)^2 + 0.208(A_1)^3 & \text{if } (A_1) \le -0.25 \\ 1.076 + 1.812(A_1) - 5.796(A_1)^2 + 4.942(A_1)^3 & \text{if } (A_1) > -0.25 \end{cases}$$

[4]
$$\Phi_2 = \begin{cases} -2.649 + 78.163(A_2) + 381.681(A_2)^2 - 15547.789(A_2)^3 & \text{if } (A_2) \le 0.05 \\ -0.927 + 39.165(A_2) - 321.743(A_2)^2 - 877.365(A_2)^3 & \text{if } (A_2) > 0.05 \end{cases}$$

$$A_1 = 0.36539x_1 - 0.01440x_2 - 0.04566x_3 + 0.85799x_4 - 0.35545x_5 + 0.04123x_6$$

$$A_2 = 0.23203x_1 + 0.01107x_2 - 0.00427x_3 - 0.97246x_4 + 0.01825x_5 - 0.00230x_6$$

$$X = [x_1, x_2, x_3, x_4, x_5, x_6] = \left[\frac{a}{l}, \frac{L}{l}, \frac{h}{a}, \frac{a/l}{L/l}, \frac{ah}{la}, \frac{L/l}{h/a}\right]$$

where the number of observations is $N = 432$, the coefficient of determination is $R^2 = 0.9988$, and the standard error of the estimation is SEE = 0.008745 (statistics); $0.05 \le a/l \le 0.5$, $0.5 \le h/a \le 6.0$, $2 \le L/l \le 7$, and $W/l = L/l$ (limits); $R_{3\text{-D}}$ is the adjustment factor for finite slab length and width using 3-D FEM analysis; Φ_1 and Φ_2 are nonparametric transformation functions of the projected lengths $a_m{}^T x$; A1 and A2 are the projected lengths $a_m{}^T x$;

Table 2. Identification and verification of dimensionless variables (edge loading).

h/a	a/l	L/l	W/l	C (cm)	a (cm)	h (cm)	l (cm)	L (m)	W (m)	E (GPa)	k (MN/m^3)	p (kPa)	P (kN)	σ (kPa)	δ (mm)	$\sigma h^2/P$	$\delta kl^2/P$
1.0	0.3	7	7	12.7	7.2	7.2	23.9	1.67	1.67	13.78	132.2	482.3	7.8	2800.1	0.37252	1.84808	0.36277
1.0	0.3	7	7	19.1	10.7	10.7	35.8	2.51	2.51	10.34	66.1	620.1	22.5	3600.7	0.95799	1.84795	0.36283
1.0	0.3	7	7	19.1	10.7	10.7	35.8	2.51	2.51	13.78	88.1	551.2	20.0	3200.4	0.63863	1.84782	0.36281
1.0	0.3	7	7	25.4	14.3	14.3	47.8	3.34	3.34	24.12	115.7	689.0	44.5	3999.6	0.60818	1.84786	0.36276
1.0	0.3	7	7	25.4	14.3	14.3	47.8	3.34	3.34	31.01	148.7	1033.5	66.8	5999.8	0.70952	1.84796	0.36275
1.0	0.3	7	7	31.8	17.9	17.9	59.7	4.18	4.18	20.67	79.3	895.7	90.4	5200.6	1.15308	1.84796	0.36280
1.0	0.3	7	7	31.8	17.9	17.9	59.7	4.18	4.18	27.56	105.7	413.4	41.7	2400.5	0.39914	1.84813	0.36279
1.0	0.3	7	7	38.1	21.5	21.5	71.7	5.02	5.02	13.78	44.1	826.8	120.2	4799.6	1.91572	1.84786	0.36275
1.0	0.3	7	7	38.1	21.5	21.5	71.7	5.02	5.02	41.34	132.2	620.1	90.1	3600.0	0.47892	1.84803	0.36274
1.0	0.3	7	7	38.1	21.5	21.5	71.7	5.02	5.02	27.56	88.1	689.0	100.1	4000.3	0.79822	1.84818	0.36275
1.5	0.2	7	7	12.7	7.2	10.7	35.8	2.51	2.51	13.78	88.1	482.3	7.8	1578.5	0.27178	2.34354	0.39703
1.5	0.2	7	7	19.1	10.7	16.1	53.7	3.76	3.76	10.34	44.1	620.1	22.5	2029.1	0.69878	2.34346	0.39696
1.5	0.2	7	7	19.1	10.7	16.1	53.7	3.76	3.76	13.78	58.7	551.2	20.0	1803.8	0.46584	2.34366	0.39695
1.5	0.2	7	7	25.4	14.3	21.5	71.7	5.02	5.02	24.12	77.1	689.0	44.5	2254.4	0.44366	2.34348	0.39695
1.5	0.2	7	7	25.4	14.3	21.5	71.7	5.02	5.02	31.01	99.1	1033.5	66.8	3381.6	0.51758	2.34348	0.39692
1.5	0.2	7	7	31.8	17.9	26.9	89.6	6.27	6.27	20.67	52.9	895.7	90.4	2931.0	0.84107	2.34382	0.39695
1.5	0.2	7	7	31.8	17.9	26.9	89.6	6.27	6.27	27.56	70.5	413.4	41.7	1352.5	0.29113	2.34336	0.39694
1.5	0.2	7	7	38.1	21.5	32.2	107.5	7.52	7.52	13.78	29.4	826.8	120.2	2705.7	1.39756	2.34366	0.39696
1.5	0.2	7	7	38.1	21.5	32.2	107.5	7.52	7.52	41.34	88.1	620.1	90.1	2029.1	0.34938	2.34346	0.39695
1.5	0.2	7	7	38.1	21.5	32.2	107.5	7.52	7.52	27.56	58.7	689.0	100.1	2254.4	0.58232	2.34330	0.39697
3.0	0.1	7	7	12.7	7.2	21.5	71.7	5.02	5.02	13.78	44.1	482.3	7.8	506.7	0.15052	3.00978	0.43975
3.0	0.1	7	7	19.1	10.7	32.2	107.5	7.52	7.52	10.34	22.0	620.1	22.5	651.5	0.38707	3.00981	0.43977
3.0	0.1	7	7	19.1	10.7	32.2	107.5	7.52	7.52	13.78	29.4	551.2	20.0	579.1	0.25804	3.00969	0.43976
3.0	0.1	7	7	25.4	14.3	43.0	143.3	10.03	10.03	24.12	38.6	689.0	44.5	724.1	0.24575	3.01100	0.43977
3.0	0.1	7	7	25.4	14.3	43.0	143.3	10.03	10.03	31.01	49.6	1033.5	66.8	1085.9	0.28672	3.01005	0.43977
3.0	0.1	7	7	31.8	17.9	53.7	179.1	12.54	12.54	20.67	26.4	895.7	90.4	941.2	0.46591	3.01020	0.43978
3.0	0.1	7	7	31.8	17.9	53.7	179.1	12.54	12.54	27.56	35.2	413.4	41.7	434.3	0.16127	3.00991	0.43977
3.0	0.1	7	7	38.1	21.5	64.5	215.0	15.05	15.05	13.78	14.7	826.8	120.2	868.8	0.77409	3.01053	0.43975
3.0	0.1	7	7	38.1	21.5	64.5	215.0	15.05	15.05	41.34	44.1	620.1	90.1	651.4	0.19353	3.00973	0.43975
3.0	0.1	7	7	38.1	21.5	64.5	215.0	15.05	15.05	27.56	29.4	689.0	100.1	724.1	0.32255	3.01100	0.43977
6.0	0.2	7	7	12.7	7.2	43.0	35.8	2.51	2.51	13.78	5639.9	482.3	7.8	60.2	0.01042	1.42950	0.97465
6.0	0.2	7	7	19.1	10.7	64.5	53.7	3.76	3.76	10.34	2820.0	620.1	22.5	77.4	0.02680	1.42990	0.97454
6.0	0.2	7	7	19.1	10.7	64.5	53.7	3.76	3.76	13.78	3760.0	551.2	20.0	68.8	0.01787	1.42944	0.97456
6.0	0.2	7	7	25.4	14.3	86.0	71.7	5.02	5.02	24.12	4934.9	689.0	44.5	86.0	0.01702	1.43007	0.97459
6.0	0.2	7	7	25.4	14.3	86.0	71.7	5.02	5.02	31.01	6344.9	1033.5	66.8	128.9	0.01986	1.42931	0.97456
6.0	0.2	7	7	31.8	17.9	107.5	89.6	6.27	6.27	20.67	3384.0	895.7	90.4	111.8	0.03227	1.42974	0.97466
6.0	0.2	7	7	31.8	17.9	107.5	89.6	6.27	6.27	27.56	4512.0	413.4	41.7	51.6	0.01117	1.42951	0.97461
6.0	0.2	7	7	38.1	21.5	129.0	107.5	7.52	7.52	13.78	1880.0	826.8	120.2	103.1	0.05361	1.42953	0.97459
6.0	0.2	7	7	38.1	21.5	129.0	107.5	7.52	7.52	41.34	5639.9	620.1	90.1	77.4	0.01340	1.42984	0.97458
6.0	0.2	7	7	38.1	21.5	129.0	107.5	7.52	7.52	27.56	3760.0	689.0	100.1	86.0	0.02234	1.43010	0.97460
3.0	0.1	2	2	12.7	7.2	21.5	71.7	1.43	1.43	13.78	44.1	482.3	7.8	403.8	0.34912	2.39833	1.01996
3.0	0.1	2	2	19.1	10.7	32.2	107.5	2.15	2.15	10.34	22.0	620.1	22.5	519.2	0.89771	2.39836	1.01994

Table 2 (*concluded*).

h/*a*	*a*/*l*	*L*/*l*	*W*/*l*	*C* (cm)	*a* (cm)	*h* (cm)	*l* (cm)	*L* (m)	*W* (m)	*E* (GPa)	*k* (MN/m^3)	*p* (kPa)	*P* (kN)	σ (kPa)	δ (mm)	$\sigma h^2/P$	$\delta k l^2/P$
3.0	0.1	2	2	19.1	10.7	32.2	107.5	2.15	2.15	13.78	29.4	551.2	20.0	461.5	0.59845	2.39844	1.01990
3.0	0.1	2	2	25.4	14.3	43.0	143.3	2.87	2.87	24.12	38.6	689.0	44.5	576.8	0.56998	2.39849	1.01996
3.0	0.1	2	2	25.4	14.3	43.0	143.3	2.87	2.87	31.01	49.6	1033.5	66.8	865.4	0.66497	2.39887	1.01996
3.0	0.1	2	2	31.8	17.9	53.7	179.1	3.58	3.58	20.67	26.4	895.7	90.4	749.6	1.08059	2.39758	1.01998
3.0	0.1	2	2	31.8	17.9	53.7	179.1	3.58	3.58	27.56	35.2	413.4	41.7	346.1	0.37404	2.39828	1.01995
3.0	0.1	2	2	38.1	21.5	64.5	215.0	4.30	4.30	13.78	14.7	826.8	120.2	692.4	1.79540	2.39935	1.01994
3.0	0.1	2	2	38.1	21.5	64.5	215.0	4.30	4.30	41.34	44.1	620.1	90.1	519.1	0.44884	2.39824	1.01992
3.0	0.1	2	2	38.1	21.5	64.5	215.0	4.30	4.30	27.56	29.4	689.0	100.1	576.8	0.74811	2.39849	1.01996
6.0	0.2	3	3	12.7	7.2	43.0	35.8	1.07	1.07	13.78	5639.9	482.3	7.8	58.9	0.01192	1.39905	1.11480
6.0	0.2	3	3	19.1	10.7	64.5	53.7	1.61	1.61	10.34	2820.0	620.1	22.5	75.7	0.03066	1.39934	1.11472
6.0	0.2	3	3	19.1	10.7	64.5	53.7	1.61	1.61	13.78	3760.0	551.2	20.0	67.3	0.02044	1.39936	1.11469
6.0	0.2	3	3	25.4	14.3	86.0	71.7	2.15	2.15	24.12	4934.9	689.0	44.5	84.1	0.01947	1.39913	1.11472
6.0	0.2	3	3	25.4	14.3	86.0	71.7	2.15	2.15	31.01	6344.9	1033.5	66.8	126.2	0.02271	1.39875	1.11470
6.0	0.2	3	3	31.8	17.9	107.5	89.6	2.69	2.69	20.67	3384.0	895.7	90.4	109.3	0.03691	1.39888	1.11475
6.0	0.2	3	3	31.8	17.9	107.5	89.6	2.69	2.69	27.56	4512.0	413.4	41.7	50.5	0.01278	1.39915	1.11475
6.0	0.2	3	3	38.1	21.5	129.0	107.5	3.22	3.22	13.78	1880.0	826.8	120.2	100.9	0.06132	1.39897	1.11472
6.0	0.2	3	3	38.1	21.5	129.0	107.5	3.22	3.22	41.34	5639.9	620.1	90.1	75.7	0.01533	1.39929	1.11472
6.0	0.2	3	3	38.1	21.5	129.0	107.5	3.22	3.22	27.56	3760.0	689.0	100.1	84.1	0.02555	1.39916	1.11470

and $\sigma_{3\text{-D FEM}}$ is the critical edge stress obtained by 3-D FEM analysis.

Jointed concrete pavements consist of many single finite concrete slabs jointed by aggregate interlock, dowel bars, or tie bars. Traffic loading may be in the form of dual, tandem, or tridem axles. A widened outer lane may also shift the wheel loading away from Westergaard's critical loading locations. A tied concrete shoulder and a second bonded or unbonded layer may also result in different degrees of stress reduction. The effect of a temperature differential or moisture gradient (linear or nonlinear) may alter the magnitude of critical stresses. Thorough treatments of various combinations of all such conditions are very challenging due to the complexity and vast amount of required computation time in 3-D FEM analysis.

A possible but aggressive approach to this problem may be to make the best use of the existing 2-D FEM research findings (Lee 1999) and strive to integrate them with new 3-D FEM results, since adjustment factors are simply defined as a proportional relationship of the results of a specified condition with those of an ideal condition. Thus, the following tentative stress equation may be used to estimate critical edge stress (σ_e) in a mechanistic design procedure, though its applicability should be further verified and adjusted if necessary:

$$[5] \qquad \sigma_e = \sigma_{we} R_{3\text{-}D} R_G R_S R_O R_M + R_T \sigma_c$$

where σ_c is the Westergaard–Bradbury edge curling solution; $R_{3\text{-}D}$ is an adjustment factor for finite slab length and width using 3-D FEM analysis; and the remaining adjustment factors still remain as the same existing 2-D FEM findings, in which R_G is the adjustment factor for different gear configurations (including dual-wheel, tandem axle, and tridem axle). R_S is the adjustment factor for a tied concrete shoulder. R_O is the adjustment factor for a widened outer lane. R_M is the adjustment factor for a bonded–unbonded second layer, and R_T is the adjustment factor for the combined effect of loading plus daytime curling.

Conclusions and recommendations

In-depth parameter studies and verifications were conducted on 3-D ABAQUS finite element analysis of rigid pavements. A systematic analytical approach was utilized and implemented in a Visual Basic software package to automatically conduct the analyses for consistency and efficiency consideration. For all three loading conditions analyzed, the resulting deflections are generally in the following descending order: ABAQUS 3-D solid elements, ABAQUS 3-D shell elements, ILLI-SLAB element, and Westergaard solutions.

The deflection convergence characteristics of eight- and nine-node elements are more effective than those of four-node elements. Generally speaking, with the exception of element types C3D8, C3D8R, and C3D27R, the deflections of all 3D shell and solid elements tend to increase to convergence when a finer horizontal and (or) vertical mesh is used. The stresses of eight- and nine-node shell elements tend to decrease to convergence, whereas the stresses of four-node shell elements increase to convergence with a finer horizontal mesh. The interior and edge stresses of element types

C3D20 and C3D27 increase to convergence at a faster rate than any other 3D solid elements when a finer vertical mesh was used.

By increasing the horizontal and vertical mesh fineness, the resulting deflections of eight-node solid elements are very close to those of 20- and 27-node elements; however, the resulting eight-node stresses are very different from those of 20- and 27-node elements. Using vertical mesh fineness of one (or one layer) proved to be inadequate and should be avoided for 3-D solid elements. In addition, using 3-D solid elements for corner stress analysis may be problematic and should be further investigated due to their poor vertical convergence characteristics.

The vertical mesh fineness was defined as the number of evenly divided slab layers for simplicity and practical model building concerns in this study. It was found that a certain aspect ratio in the vertical direction, e.g., less than 0.8 as recommended by previous literature, may be too burdensome. To achieve high accuracy and computational efficiency, the selection of element types C3D20 or C3D27 with a horizontal mesh fineness of three and a vertical mesh fineness of three may be adequate.

Similar conclusions were reached for mesh fineness and element selection study using different slab thicknesses (h/a) and load sizes (a/l). The deflections and stresses of ILLI-SLAB and four-node elements were affected by the length of zone II, whereas the differences in deflections and stresses due to the selection of nC are limited or negligible for 3-D shell and solid elements. Thus, a value of three times C was recommended for all element types for consistency and conservative consideration.

An additional dominating dimensionless variable (h/a) defined as the ratio of slab thickness (h) to load radius (a) was identified and verified to have a substantial influence on ABAQUS runs using either 3-D shell or solid elements. Together with the normalized load radius (a/l), the normalized finite slab length (L/l), and the normalized finite slab width (W/l), this additional mechanistic variable can be used to account for the differences among various 2-D and 3-D FEM idealizations and theoretical closed-form stress and deflection solutions. Separate stress and deflection databases were created using these four variables for the C3D27 element. An example critical stress predictive model in terms of adjustment factors was presented to illustrate their possible applications, since adjustment factors are simply defined as a proportional relationship of the results of a specified condition to those of an ideal condition. Together with the existing 2-D FEM research findings, a tentative stress prediction equation was proposed and should be subjected to further verifications.

Acknowledgements

This study was sponsored by the National Science Council, Taiwan. This paper presents some excerpts from the M.S. thesis of Mr. Hsin-Ta Wu. Mr. Shao-Tang Yen consistently provided fruitful technical assistance in 3-D ABAQUS analyses. Dr. Chen-Ming Kuo and Dr. Ping-Sien Lin are gratefully acknowledged for their helpful guidance and recommendations.

References

Brill, D.R. 1998. Development of advanced computational models for airport pavement design. Final Report, DOT/FAA/AR-97/47, US Department of Transportation, Federal Aviation Administration, Washington, D.C.

Burmister, D.M. 1943. The theory of stresses and displacements in layered systems and applications to the design of airport runways. Proceedings of the Annual Meeting of the Highway Research Board, **23**: 126–144.

Burmister, D.M. 1945. The general theory of stresses and displacements in layered soil systems. Journal of Applied Physics, **16**: 84–94, 126–127, 296–302.

Friedman, J.H., and Stuetzle, W. 1981. Projection pursuit regression. Journal of the American Statistical Association, **76**: 817–823.

Hammons, M.I. 1998. Advanced pavement design: finite element modeling for rigid pavement joints. Report II: model development, DOT/FAA/AR-97-7, US Department of Transportation, Federal Aviation Administration, Washington, D.C.

Hibbitt, Karlsson, & Sorensen, Inc. 2000. ABAQUS/standard user's manual. Vols. I and II. Hibbitt, Karlsson, & Sorensen, Inc., Pawtucket, R.I.

Huang, Y.H. 1993. Pavement analysis and design. Prentice-Hall Inc., Englewood Cliffs, N.J.

Ioannides, A.M. 1984. Analysis of slabs-on-grade for a variety of loading and support conditions. Ph.D. dissertation, University of Illinois, Urbana, Ill.

Ioannides, A.M., and Khazanovich, L. 1994. Analytical and numerical methods for multi-layered concrete pavements. *In* Proceedings of the 3rd International Workshop on the Theoretical Design of Evaluation of Concrete Pavements, Krumbach, Austria, 29–30 September 1994. Centre for Research and Contract Standardization in Civil and Traffic Engineering, The Netherlands. pp. 113–121.

Ioannides, A.M., and Salsilli-Murua, R.A. 1989. Temperature curling in rigid pavements: an application of dimensional analysis. *In* Transportation Research Record 1227. Transportation Research Board, National Research Council (US), Washington, D.C. pp. 1–11.

Ioannides, A.M., Thompson, M.R., and Barenberg, E.J. 1985. Westergaard solution reconsidered. *In* Transportation Research Record 1043. Transportation Research Board, National Research Council (US), Washington, D.C. pp. 12–23.

Khazanovich, L., and Ioannides, A.M. 1995. DIPLOMAT: analysis program for bituminous and concrete pavements. *In* Transportation Research Record 1482. Transportation Research Board, National Research Council (US), National Academy Press, Washington, D.C. pp. 52–60.

Kim, J., and Hjelmstad, K. 2000. Three-dimensional finite element analysis of multi-layered systems: comprehensive nonlinear analysis of rigid airport pavement systems. Technical Report of Research supported by the Federal Aviation Administration under Grant DOT95-C-001.

Korovesis, G.T. 1990. Analysis of slab-on-grade pavement systems subjected to wheel and temperature loadings. Ph.D. dissertation, University of Illinois, Urbana, Ill.

Kuo, C.M. 1994. Three-dimensional finite element model for analysis of concrete pavement support. Ph.D. dissertation, University of Illinois, Urbana, Ill.

Lee, Y.H. 1993. Development of pavement prediction models. Ph.D. dissertation, University of Illinois, Urbana, Ill.

Lee, Y.H. 1999. TKUPAV: stress analysis and thickness design program for rigid pavements. ASCE Journal of Transportation Engineering, **125**(4): 338–346.

Lee, Y.H., and Darter, M.I. 1994. New predictive modeling techniques for pavements. *In* Transportation Research Record 1449. Transportation Research Board, National Research Council (US), National Academy Press, Washington, D.C. pp. 234–245.

Salsilli-Murua, R.A. 1991. Calibrated mechanistic design procedure for jointed plain concrete pavements. Ph.D. dissertation, University of Illinois, Urbana, Ill.

Shi, X., and Yao, Z. 1989. Concrete pavement design procedure for container terminals. *In* Proceedings of the 4th International Conference on Concrete Pavement Design and Rehabilitation, 18–20 April 1989. Purdue University, West Lafayette, Ind. pp. 53–59.

Thompson, M.R., and Navneet, G. 1999. Wheel load interaction: critical airport pavement responses. Technical Report of Research supported by the Federal Aviation Administration under Grant DOT95-C-001.

Van Cauwelaert, F. 1990. Westergaard equations for thick elastic plates. *In* Proceedings of the 2nd International Workshop on the Theoretical Design of Concrete Pavements, Sigüenza, Spain, 4–5 October 1990. Centre for Research and Contract Standardization in Civil and Traffic Engineering, The Netherlands. pp. 165–175.

Wu, H.-T. 2003. Parameter analysis and verification for jointed concrete pavements. M.S. thesis, Tamkang University, Tamsui, Taiwan. [In Chinese.]

List of symbols

a radius of the applied load

A_1, A_2 projected lengths $a_m^T x$

C length of loaded area

E concrete modulus of the slab

h thickness of the slab

k modulus of subgrade reaction

l radius of relative stiffness of the slab–subgrade system

L finite slab length

n multiplier

N number of observations

p tire pressure

P single wheel load

$R_{3\text{-}D}$ adjustment factor for finite slab length and width using 3-D FEM analysis

R^2 coefficient of determination

R_G adjustment factor for different gear configurations including dual-wheel, tandem axle, and tridem axle

R_M adjustment factor for a bonded–unbonded second layer

R_O adjustment factor for a widened outer lane

R_S adjustment factor for a tied concrete shoulder

R_T adjustment factor for the combined effect of loading plus daytime curling

SEE standard error of the estimation

W finite slab width

$x_1, x_2, x_3, x_4, x_5, x_6$ vector of predictor variables

δ slab deflection

δ_{we}, δ_{wi}, δ_{wc} edge, interior, and corner deflections

γ Euler's constant

μ Poisson's ratio

σ slab bending stress

σ_c Westergaard–Bradbury edge curling solution

σ_e critical edge stress

$\sigma_{3\text{-}DFEM}$ critical edge stress obtained by 3-D FEM analysis

σ_{we}, σ_{wi}, σ_{wc} Westergaard's closed-form edge, interior, and corner stress solutions

Φ_1, Φ_2 nonparametric transformation functions of the projected lengths $a_m^T x$

Fig. 10. Edge stress convergence study due to the length of neighborhood area.

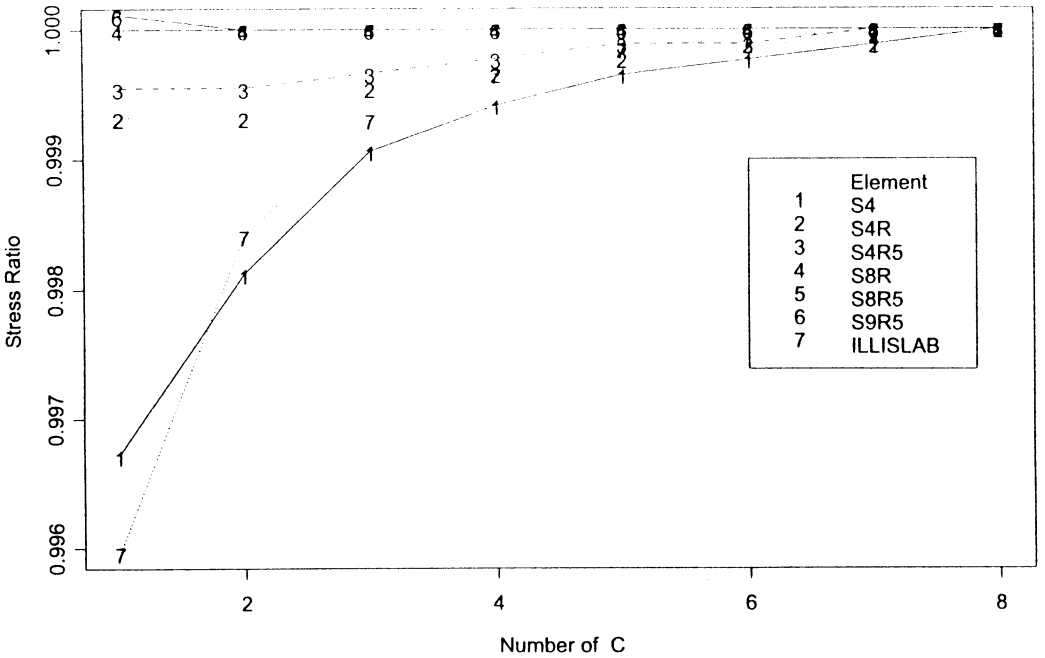

highway and airfield rigid pavement conditions. Separate deflection and stress databases were created for all three loading conditions using element type C3D27 with a horizontal mesh fineness of three, a vertical mesh fineness of three, and the same finer mesh extended to three times the length of the loaded area (C).

Deflection ratios and stress ratios defined as the ratio of 3-D finite element results to Westergaard solutions were calculated while assuming the normalized slab width W/l equals L/l, i.e., square slabs. Note that Westergaard's closed-form solutions only serve as benchmarks herein instead of "exact solutions," since the solutions are based on the simplification that ignores plate compressibility and shear deformation. Since the resulting deflection ratios always had a value greater than 1, their reciprocals or adjustment factors (R) will range from 0 to 1. The very high deflection ratios occurred when a thicker pavement (larger h/a) or a larger load size (larger a/l) was analyzed. Similarly, the resulting edge stress ratios ranged from 0.25 to 1.03.

To illustrate possible applications of these databases, the following predictive model was developed for critical edge stress estimation using the projection pursuit regression technique (Lee and Darter 1994; Friedman and Stuetzle 1981):

$$R_{3\text{-D}} = \frac{\sigma_{3\text{-DFEM}}}{\sigma_{we}} = f\left(\frac{a}{l}, \frac{L}{l}, \frac{h}{a}\right)$$

$$R_{3\text{-D}} = 0.69149 + 0.259\Phi_1 + 0.03318\Phi_2$$

$$\Phi_1 = \begin{cases} 1.578 + 6.013(A_1) + 2.673(A_1)^2 + 0.208(A_1)^3 & \text{if } (A_1) \le -0.25 \\ 1.076 + 1.812(A_1) - 5.796(A_1)^2 + 4.942(A_1)^3 & \text{if } (A_1) > -0.25 \end{cases}$$

[4]
$$\Phi_2 = \begin{cases} -2.649 + 78.163(A_2) + 381.681(A_2)^2 - 15547.789(A_2)^3 & \text{if } (A_2) \le 0.05 \\ -0.927 + 39.165(A_2) - 321.743(A_2)^2 + 877.365(A_2)^3 & \text{if } (A_2) > 0.05 \end{cases}$$

changed to $+877.365(A_2)^3$

$$A_1 = 0.36539x_1 - 0.01440x_2 - 0.04566x_3 + 0.85799x_4 - 0.35545x_5 + 0.04123x_6$$

$$A_2 = 0.23203x_1 + 0.01107x_2 - 0.00427x_3 - 0.97246x_4 + 0.01825x_5 - 0.00230x_6$$

$$X = [x_1, x_2, x_3, x_4, x_5, x_6] = \left[\frac{a}{l}, \frac{L}{l}, \frac{h}{a}, \frac{a/l}{L/l}, \frac{ah}{la}, \frac{L/l}{h/a}\right]$$

where the number of observations is $N = 432$, the coefficient of determination is $R^2 = 0.9988$, and the standard error of the estimation is SEE = 0.008745 (statistics); $0.05 \le a/l \le 0.5$, $0.5 \le h/a \le 6.0$, $2 \le L/l \le 7$, and $W/l = L/l$ (limits); $R_{3\text{-D}}$ is the adjustment factor for finite slab length and width using 3-D FEM analysis; Φ_1 and Φ_2 are nonparametric transformation functions of the projected lengths $a_m{}^T x$; A1 and A2 are the projected lengths $a_m{}^T x$;